J. Cent. South Univ. (2021) 28: 3778−3789
DOI: https://doi.org/10.1007/s11771-021-4847-y

Springer

Ferroelectric polarization-enhanced photocatalytic performance of heterostructured $BaTiO_3$@TiO_2 via interface engineering

FAN Bao-yan(范保艳)[1], LIU Hai-bo(刘海波)[1], WANG Zhen-hui(王振慧)[1], ZHAO Yi-wen(赵夷雯)[1], YANG Sen(杨森)[1], LYU Si-yi(吕思宜)[1], XING An(邢安)[1], ZHANG Jun(张均)[1], LI He(李禾)[2], LIU Xiao-yan(刘晓燕)[1]*

1. Chongqing Key Laboratory of Nano/Micro Composites and Devices, College of Metallurgy and Materials Engineering, Chongqing University of Science and Technology, Chongqing 401331, China;
2. The Molecular Foundry, Lawrence Berkeley National Laboratory, Berkeley, California 94720, USA

Abstract: A catalyst of ferroelectric-$BaTiO_3$@photoelectric-TiO_2 nanohybrids ($BaTiO_3$@TiO_2) with enhanced photocatalytic activity was synthesized via a hydrolysis precipitation combined with a hydrothermal approach. Compared to pure TiO_2, pure $BaTiO_3$ and $BaTiO_3$/TiO_2 physical mixture, the heterostructured $BaTiO_3$@TiO_2 exhibits significantly improved photocatalytic activity and cycling stability in decomposing Rhodamine B (RhB) and the degradation efficiency is 1.7 times higher than pure TiO_2 and 7.2 times higher than pure $BaTiO_3$. These results are mainly attributed to the synergy effect of photoelectric TiO_2, ferroelectric-$BaTiO_3$ and the rationally designed interfacial structure. The mesoporous microstructure of TiO_2 is of a high specific area and enables excellent photocatalytic activity. The ferroelectric polarization induced built-in electric field in $BaTiO_3$ nanoparticles, and the intimate interfacial interactions at the interface of $BaTiO_3$ and TiO_2 are effective in driving the separation and transport of photogenerated charge carriers. This strategy will stimulate the design of heterostructured photocatalysts with outstanding photocatalytic performance via interface engineering.

Key words: heterostructured $BaTiO_3$@TiO_2; ferroelectric polarization; interfacial interactions; photocatalytic activity

Cite this article as: FAN Bao-yan, LIU Hai-bo, WANG Zhen-hui, ZHAO Yi-wen, YANG Sen, LYU Si-yi, XING An, ZHANG Jun, LI He, LIU Xiao-yan. Ferroelectric polarization-enhanced photocatalytic performance of heterostructured $BaTiO_3$@TiO_2 via interface engineering [J]. Journal of Central South University, 2021, 28(12): 3778−3789. DOI: https://doi.org/10.1007/s11771-021-4847-y.

1 Introduction

The increasing organic wastewater has brought serious environmental pollution and health issues, and thus attracts substantial interest in decomposing and purifying wastewater [1−4]. Semiconductor photocatalysis is considered as one of the most promising techniques to address environmental pollution and energy demands, in which solar energy can be directly converted into chemical energy for organic wastewater decomposition [5, 6]. The semiconductor photocatalysis process mainly contains generation and transportation of charge carriers under light irradiation, which would further

Foundation item: Project(cstc2020jcyj-msxmX0930) supported by the Natural Science Foundation of Chongqing, China; Project (KJQN201901522) supported by Technological Research Program of Chongqing Municipal Education Commission, China; Project(cx2020068) supported by the Venture & Innovation Support Program for Chongqing Overseas Returnees, China
Received date: 2021-06-23; **Accepted date:** 2021-10-09
Corresponding author: LIU Xiao-yan, PhD, Professor; E-mail: xyliu@cqust.edu.cn; ORCID: https://orcid.org/0000-0002-2070-0798

react with water to induce actives including hydroxyl radicals (OH•) and superoxide anions ($•O_2^-$) to decompose organic pollutants [7]. An efficient photocatalyst should possess the characteristic of broad optical adsorption range, effective charge-carrier separation, and good chemical stability [8]. Among various semiconductor photocatalysts, such as ZnO [9], Fe_3O_4 [10], WO_3 [11] and CdS [12], TiO_2 is one of the potential photocatalysts which are widely studied due to their strong catalytic oxidation, non-toxic feature and low price [13]. Moreover, the large specific area of mesoporous TiO_2 nanoparticles is another favorable factor for generating large quantities of active sites for photocatalytic reaction, which has been taken place on the surface of photocatalyst [14]. However, photogenerated charge carriers are loosely bound by the Coulomb force and tend to recombine within femtoseconds, resulting in low quantum yield of TiO_2 and limited photocatalytic efficiency due to the low transfer rate of surface charge carriers and quick recombination rate of electron-hole pairs [15]. Furthermore, great efforts have been exploited to in-situ synthesis of heterostructured photocatalysts to reinforce interfacial interactions and boost more efficient carrier transfer [16, 17].

Recently, heterostructured ferroelectric photocatalysts have been widely reported. The ferroelectric polarization-induced built-in electric field causes a mismatch in the electrochemical potential of surface electrons, which accelerates separation and migration of photogenerated carriers in opposite directions. The built-in electric field drives the separation of holes and electrons, resulting in inhibiting the recombination of charge carriers and prolonging the lifetime. Heterostructured photocatalysts composed of ferroelectrics core and nanostructured TiO_2 shell displayed an improving photocatalytic activity for hydrogen production and organic pollutants degradation [18, 19]. Large polarization renders the typical ferroelectric $BaTiO_3$ as a promising candidate to construct a heterojunction combined with TiO_2. The ferroelectric polarization-induced built-in electric field at the interface will drive the transfer and separation of charge carriers. FENG et al [20] and YANG et al [21] validated the positive effect of built-in electric field on suppressing charge recombination in dye-sensitized solar cells and photoelectrochemical photoanodes, respectively. HUANG et al [22] demonstrated that heterostructured PZT/TiO_2 possesses efficient photocatalytic activities with high photochemical stability under visible light irradiation. WANG et al [23] and SU et al [24] succeeded in synthesizing Fe_3O_4@TiO_2-$BaTiO_3$ ferroelectric nanohybrids and $SrTiO_3$/TiO_2 nanotubes by hydrothermal method for the acquirement of highly efficient photocatalysts. In addition, ferroelectric photocatalysts have been prepared and studied intensively, e. g., core-shell-heterostructured $BaTiO_3$/Fe_3O_4 [25] and $PbTiO_3$/TiO_2 [22] nanoparticles were prepared by conventional sonochemical and sol-gel method; heterostructured $BiFeO_3$/TiO_2 [16] and (Ba, Sr)TiO_3/TiO_2 [18] were synthesized via a hydrolysis precipitation processing combined with a hydrothermal approach.

While it is well-accepted that the interfacial contact region between two phases is fundamentally related to the transfer behavior of charge carriers, and the interface structure and interfacial interaction have great effects on the efficiency of charge transfer, but little attention has been focused on the effect of interfacial interaction between ferroelectric $BaTiO_3$ and mesoporous TiO_2 on photocatalytic efficiency. In this work, a novel ferroelectric-$BaTiO_3$@photoelectric-TiO_2 photocatalyst is designed and synthesized by hydrolysis precipitation combined with a hydrothermal approach. By comparing structures and properties of $BaTiO_3$/TiO_2 physical mixtures and heterostructured $BaTiO_3$@TiO_2, the synergy effect of photoelectric TiO_2 and ferroelectric $BaTiO_3$, as well as their interfacial interactions, has been revealed. It is supposed that the ferroelectric spontaneous polarization-induced built-in electric field can act as an influential driving force for promoting the separation of photogenerated charge carriers. Furthermore, the effect of interfacial coupling between $BaTiO_3$ and TiO_2 is also clarified evidently. The photocatalytic performance of $BaTiO_3$@TiO_2 nanohybrids is largely enhanced by the heterostructure design.

2 Experimental

2.1 Materials preparation

Stöber method [26] was adopted to construct multifunctional heterostructure with ferroelectric $BaTiO_3$ core and mesoporous TiO_2 shell. $BaTiO_3$ nanoparticles (99%, Sakai Chemical Industry) with a diameter of 50−150 nm were obtained commercially. Figure 1 illustrates the synthesis process of the heterostructured $BaTiO_3$@TiO_2 photocatalysts. $BaTiO_3$ nanoparticles were ultrasonically dispersed in ethanol, followed by the addition of hexadecylamine (HDA, 90%), which acts as a surfactant to adsorb on $BaTiO_3$ surfaces and form isolated nanoparticles. Then ammonia was added and stirred at room temperature for 10 min for a homogeneous solution. Hydrolysis product (TiO_2) was obtained by the hydrolysis reaction of titanium isopropoxide (TIP, 95%). After that, a class of inorganic-organic composites ($BaTiO_3$@TiO_2/HDA) was synthesized by the reaction of TiO_2 with the amino groups in HDA molecules. The hydrophobic long carbon chains of HDA are favorable for the formation of mesoporous TiO_2 (Figure 1). The prepared products of $BaTiO_3$@TiO_2/HDA nanocomposites were centrifugally collected, washed, and then dispersed in a mixture of ethanol and DI water. The resulting mixtures were sealed in a Teflon-lined autoclave (50 mL in capacity) and heated at 160 °C for 16 h to remove the organic species. After cooling down to room temperature, the heterostructured $BaTiO_3$@TiO_2 nanohybrids were obtained. For investigating the interfacial interactions in heterostructured $BaTiO_3$@TiO_2, the optimized weight ratio of 1.2: 1 of $BaTiO_3$ to TiO_2 was selected as reported in our former studies [27]. The pristine TiO_2 was obtained by hydrolysis of TIP in the same experimental conditions. $BaTiO_3$ and TiO_2 with a weight ratio of 1.2: 1 were mixed into ethanol solution. The obtained suspensions were stirred for 0.5 h, sonicated for 12 h, and then baked at 80 °C for 10 h to obtain $BaTiO_3$/TiO_2 physical mixtures.

2.2 Characterization

X-ray diffraction (XRD, DX-2700 diffractometer) using Cu K_α radiation (35 kV-25 mA) was applied to investigate the phase structure of as-prepared products. The morphology was investigated by a high-resolution emission transmission electron microscope (HRTEM, JEM-2100F, Japan) and field-emission scanning electron microscope (FESEM, JSM-7800F, Japan). The ferroelectric nature of $BaTiO_3$ was performed by piezoresponse force microscope (PFM, Asylum Research, Cypher ™, USA) via running a phase-voltage hysteresis and amplitude-voltage butterfly loops. Quadrasorb 2MP was used to characterize the Brunauer-Emmett-Teller (BET) surface areas using N_2 as the adsorption gas. The RhB decomposition rates were figured out using a UV-vis

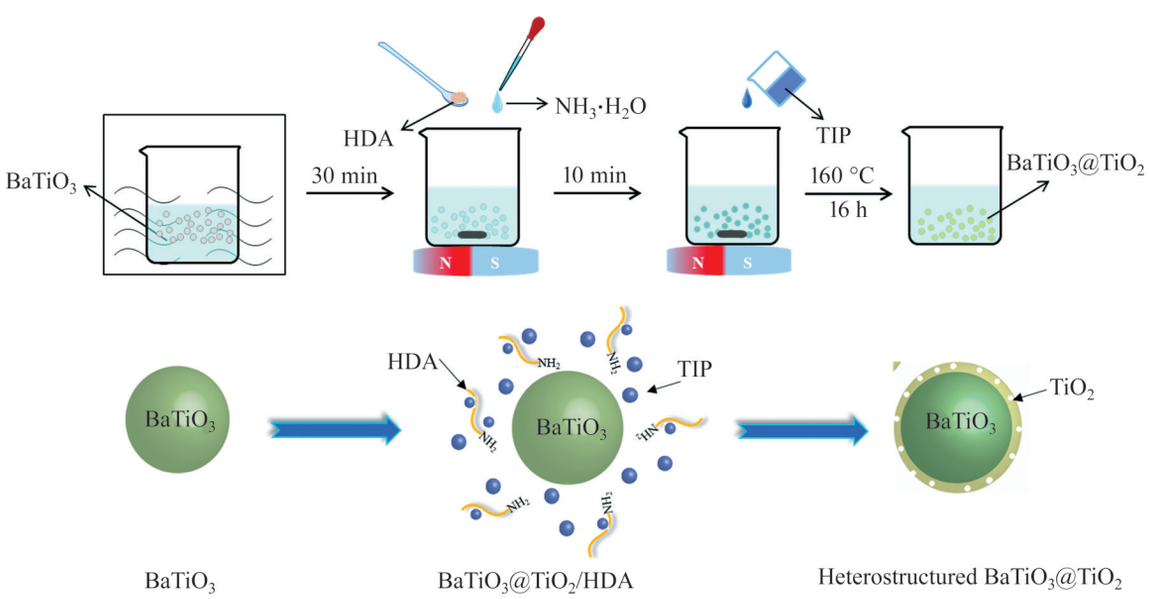

Figure 1 Schematic illustration of preparation procedure for heterostructured $BaTiO_3$@TiO_2

spectrophotometer (Persee T10, Auburn, CA, USA) to record the calibration curve with the wavelength ranging from 300 nm to 700 nm.

2.3 Photocatalytic test

RhB solution (50 mL, 15×10^{-6}) was selected to evaluate the photocatalyst activity under UV light irradiation. 30 mg as-prepared photocatalysts were dispersed in RhB solution. The mixed solution was stirred for 30 min in darkness and then transferred to a centrifuge tube which exposes to UV radiation. During the entire experimental process, a UV spotlight source (L9566-02, Hamamatsu Photonics, Japan) equipped with a 200 W mercury-xenon lamp and a 280−400 nm filter were used for the illumination. The reaction mixture of 3 mL was extracted every 30 min, and then transfer red to a centrifuge tube to remove the photocatalyst by high-speed centrifugation. The degradation rates were calculated according to the absorption spectra measured by UV-Vis spectroscopic measurements in the range of 300−700 nm.

3 Results and discussion

3.1 XRD analysis of photocatalysts

Figure 2 shows the XRD patterns of pure $BaTiO_3$, pure TiO_2, $BaTiO_3/TiO_2$ physical mixtures and heterostructured $BaTiO_3@TiO_2$. All diffraction peaks can be indexed as well-crystallized perovskite $BaTiO_3$ (JCPDS 05-0626) and anatase (JCPDS 21-1272) TiO_2. The main peaks of (110) at 31.5° can be indexed to the pure tetragonal phase of $BaTiO_3$. The

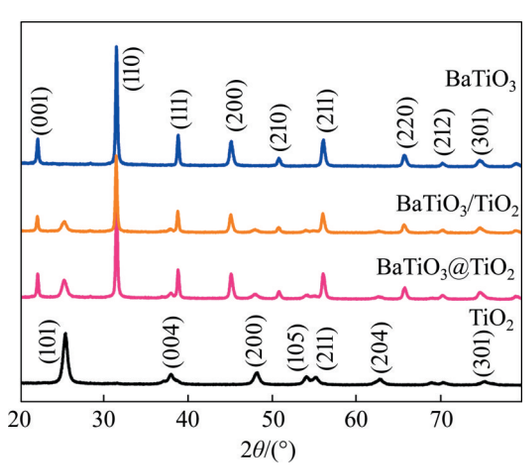

Figure 2 XRD patterns of photocatalyst of $BaTiO_3$, TiO_2, $BaTiO_3/TiO_2$ physical mixtures and heterostructured $BaTiO_3@TiO_2$

tetragonal structure and moderate size dimension (50−150 nm) endow $BaTiO_3$ possess a spontaneous polarization (P_s=27 μC/cm^2) and excellent ferroelectricity at room temperature that can induce a built-in electric field [28]. The characteristic peaks at 25.2°, 38.5° and 48.0° in the XRD spectra correspond to the characteristic planes (101), (004) and (200) of anatase TiO_2, respectively. Compared with rutile TiO_2, the formed anatase TiO_2 exhibits better photocatalytic activity due to the longer carrier lifetime [29]. No impurity peaks were observed in $BaTiO_3/TiO_2$ physical mixtures and heterostructured $BaTiO_3@TiO_2$, indicating that no secondary phases are produced between the interface of $BaTiO_3$ and TiO_2. The resulting phase structure is a benefit for gaining excellent photocatalytic performance.

3.2 Morphology of photocatalysts

Figures 3(a)−(f) present microstructures of $BaTiO_3$, TiO_2, $BaTiO_3/TiO_2$ physical mixtures and heterostructured $BaTiO_3@TiO_2$ by FESEM and HRTEM. The average diameter of pure $BaTiO_3$ and TiO_2 was around 120 nm and 430 nm, respectively. In $BaTiO_3/TiO_2$ physical mixtures, self-agglomerating $BaTiO_3$ nanoparticles tend to fill the gap formed by the spherical agglomeration of TiO_2 (Figure 3(c)). Thus, the interface between $BaTiO_3$ and TiO_2 is in random contact and easier to break and disappear, $BaTiO_3$ and TiO_2 particles exist in isolation. The composition of $BaTiO_3$ and TiO_2 can be verified by the energy dispersive X-ray spectrometry (EDS) spectra (Figures 3(g) and (h). Unlike the good dispersion and smooth surface of pure $BaTiO_3$, large aggregates and fuzzy grain boundaries are observed in heterostructured $BaTiO_3@TiO_2$ (Figure 3(d)). This is related to the characteristics of TiO_2 that nano-scale grains with mesopores generate a high surface area. Figures 3(d)−(f) show the representative structure of heterostructured $BaTiO_3@TiO_2$ by the characterization of HRTEM and indicate that TiO_2 has been coated on the surface of $BaTiO_3$ tightly. The size dimension of $BaTiO_3$ is above a critical size of 5−10 nm, which enables the ferroelectricity of $BaTiO_3$ at ambient temperature [30]. The depletion layer width less than 100 nm allows the polarization-induced built-in field to penetrate

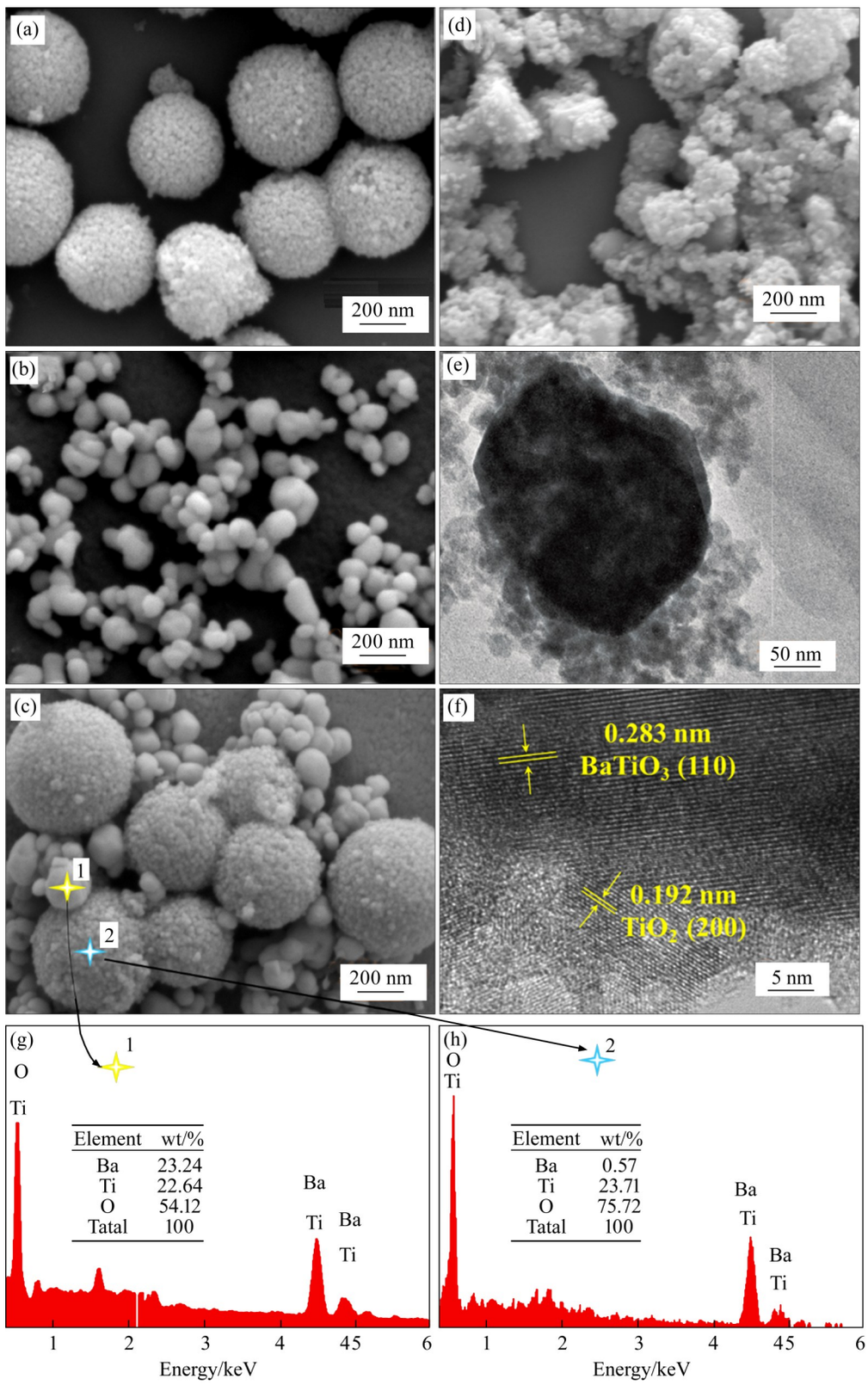

Figure 3 SEM images of TiO_2 (a), $BaTiO_3$ (b), $BaTiO_3$/TiO_2 physical mixtures (c), heterostructured $BaTiO_3$@TiO_2 (d); (e, f) FETEM images of heterostructured $BaTiO_3$@TiO_2; (g, h) EDX spectra of Position 1 and Position 2, which represent $BaTiO_3$ and TiO_2, respectively

through the interfacial layer and promote the separation of electron hole pairs (Figure 3(f)). HRTEM image in Figure 3(f) reveals the heterostructure of $BaTiO_3$@TiO_2, a lattice spacing of

0.283 nm is corresponding to the (110) plane of tetragonal $BaTiO_3$, and of 0.192 nm in agreement with the (200) plane of anatase TiO_2, which matches the XRD results. As a result, an intimate contact has been formed at the interfacial region of $BaTiO_3$ and TiO_2 in $BaTiO_3$@TiO_2 nanohybrids. Such a heterostructure possesses better mechanical strength to avoid the corruption of the interface.

3.3 Ferroelectricity of $BaTiO_3$ nanoparticles

In order to better illustrate the ferroelectric characteristics of $BaTiO_3$ in the heterostructured $BaTiO_3$@TiO_2, PFM was employed to directly examine the ferroelectricity of $BaTiO_3$ nanoparticles (Figure 4) [23]. The morphology, amplitude and phase images of $BaTiO_3$ were displayed in Figures 4(a)−(c), respectively. Spherical and agglomerated particle morphology of $BaTiO_3$ was found in morphology image and clear contrasts were detected both in amplitude and phase images of $BaTiO_3$. The obvious piezoelectric signals with alternating brightness and clear contrast are related to the domain structures of $BaTiO_3$. The amplitude and phase image testify intrinsic ferroelectric property of $BaTiO_3$ nanoparticles at room temperature. Switching spectroscopy piezoresponse force microscopy (SSPFM) loops (Figure 4(d)) subjected to DC voltage (±14.5 V) were measured to investigate the local switching behavior of $BaTiO_3$. The blue and red lines represent phase-voltage hysteresis and amplitude-voltage butterfly loops of $BaTiO_3$, respectively. A perfectly square phase-voltage hysteresis loop indicates the typical 180° domain switching and amplitude-voltage butterfly loop demonstrates the electrostrictive characteristic, further confirming the intrinsic ferroelectric property of $BaTiO_3$ [20, 31]. The SSPFM loops are shifted to negative voltage indicating that $BaTiO_3$ generates a downward oriented built-in electric field. The built-in voltage ($V_s = (V_c^+ + V_c^-)/2 = 4$ V) is calculated according to the coercive voltages ($V_c^+ \approx 10.5$ V,

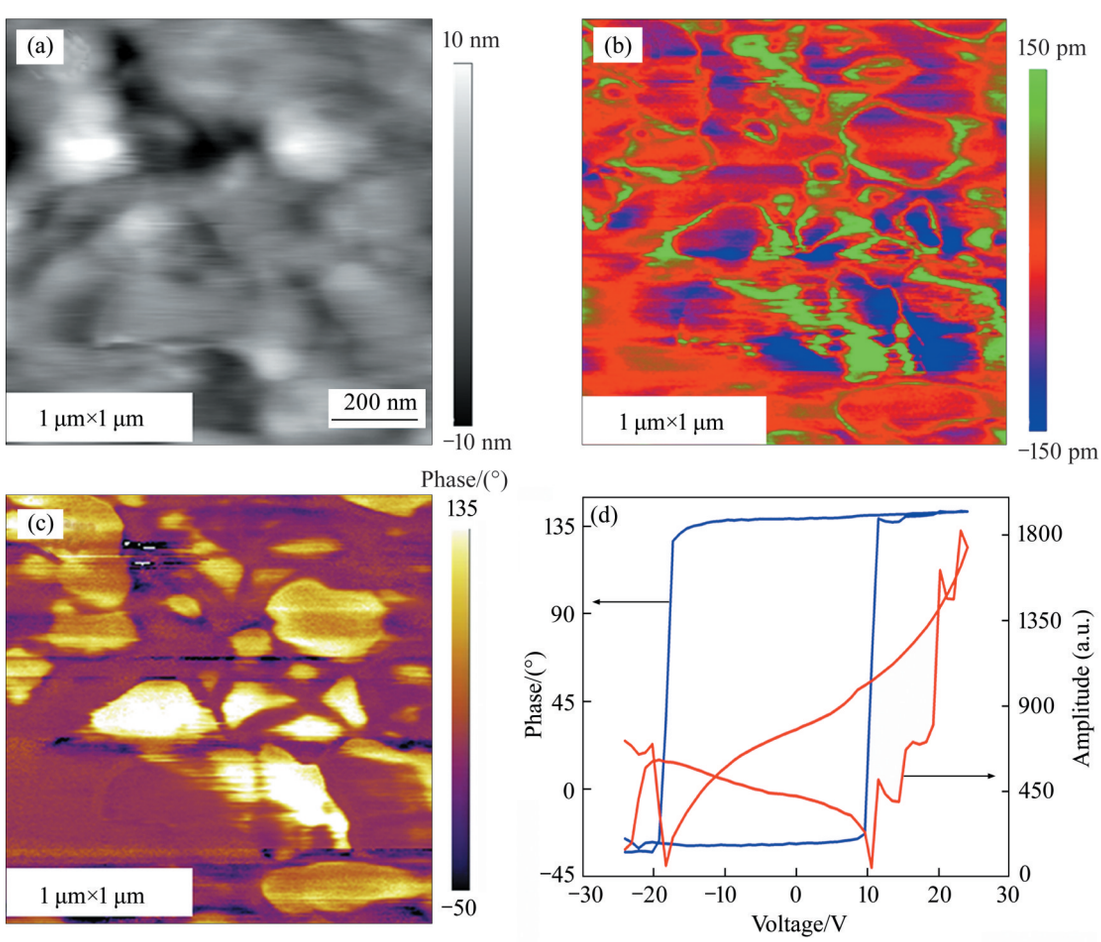

Figure 4 Characterization of ferroelectric property of $BaTiO_3$: (a) Topographic image; (b) Amplitude image; (c) Phase image; (d) Representative phase−voltage hysteresis loop (blue) and amplitude−voltage butterfly loop (red)

$V_c^- \approx -18.5$ V), which would lead to a built-in electric field and thus provide a driving force for promoting the charge carriers separation [32, 33].

3.4 Performance of photocatalysts

Photocatalysts with large BET surface areas are beneficial for generating more active sites for redox reaction, which can degrade organic pollutants. As shown in Figure 5, the BET surface area of $BaTiO_3$, TiO_2, $BaTiO_3/TiO_2$ and $BaTiO_3@TiO_2$ are 34.08 m^2/g, 73.48 m^2/g, 39.71 m^2/g and 35.77 m^2/g, respectively. The mesoporous structure of TiO_2 induces the highest BET surface area, and the pure $BaTiO_3$ with a smooth surface delivers the lowest value, whereas the median values are obtained in both $BaTiO_3/TiO_2$ physical mixtures and heterostructured $BaTiO_3@TiO_2$. $BaTiO_3@TiO_2$ with the slightly lower BET surface area possesses larger photocatalytic efficiency (Figure 6) than $BaTiO_3/TiO_2$ physical mixtures. This phenomenon can help us to reveal the paradoxical effect of decomposition efficiency (D) by designing heterostructured $BaTiO_3@TiO_2$.

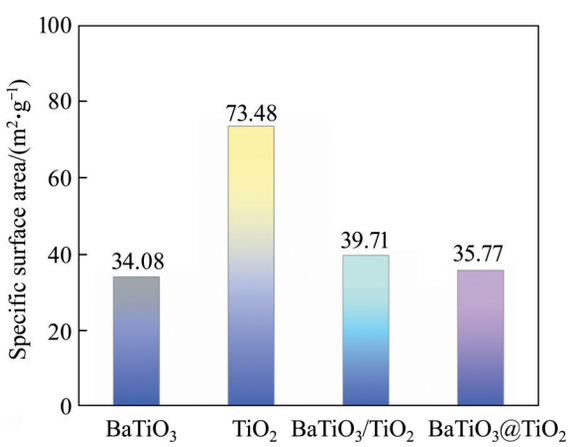

Figure 5 BET surface area of $BaTiO_3$, TiO_2, $BaTiO_3/TiO_2$ physical mixtures and heterostructured $BaTiO_3@TiO_2$

The D can be explained as: $D = (1 - C_t/C_0) * 100\%$, where C_0 and C_t are the initial and actual concentrations of RhB after performing different irradiation time intervals, respectively. To investigate the enhancement in the photocatalysis property of heterostructured $BaTiO_3@TiO_2$, D of RhB in the presence of photocatalyst $BaTiO_3$, TiO_2, $BaTiO_3/TiO_2$ physical mixtures is systematically measured for comparison (Figure 6). $BaTiO_3/TiO_2$

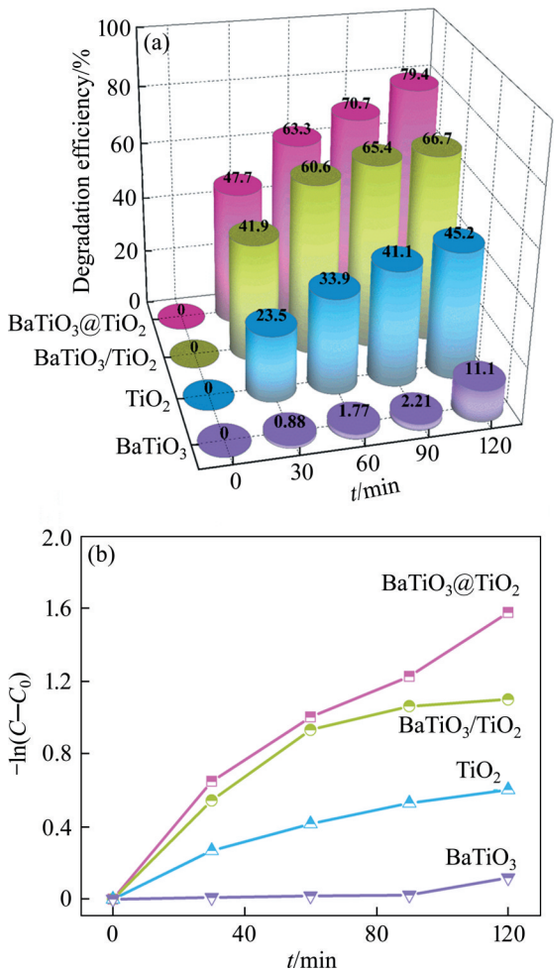

Figure 6 Comparison of decomposition efficiency (a) and degradation rate (b) of RhB with different photocatalysts under UV light irradiation

physical mixtures are composed of commercial $BaTiO_3$ and hydrothermal synthesized mesoporous TiO_2, which are prepared using the same hydrolysis reaction followed by the hydrothermal process. Figure 6(a) indicates that the D of heterostructured $BaTiO_3@TiO_2$ is the largest among the photocatalysts investigated herein. $BaTiO_3$ exhibits a slight degradation with the increasing degradation time. Only 18% of the initial wastewater was degraded under 120 min, which is supposed to be related to the smooth, low BET surface area (34.8 m^2/g) and low photocatalytic activity of $BaTiO_3$ (Figure 5). The pristine TiO_2 with a high BET surface area (73.48 m^2/g) can degrade almost 55% of the initial wastewater at the same conditions. Comparatively, both $BaTiO_3/TiO_2$ physical mixtures and heterostructured $BaTiO_3@TiO_2$ exhibit significantly higher D

compared with that of single-phase photocatalysts, which can degrade almost 67% and 80% of the initial wastewater, respectively. Ideally, when TiO_2 was physically mixed with $BaTiO_3$, the photocatalytic activity should be decreased due to the smooth surface of $BaTiO_3$, but we found an abnormal *D* increase in $BaTiO_3/TiO_2$ physical mixtures, which can be explained as following reasons. First, the weakened catalytic activity can be compensated by the cooperation effects of the increased surface area by TiO_2 deagglomeration and the polarization-induced built-in electric field by $BaTiO_3$. Second, the built-in electric field can promote the separation of generous photo-induced carriers which are related to the increased surface area. These typical results illustrate the synergistic effect of mesoporous TiO_2 and ferroelectric $BaTiO_3$. Due to the good dispersion property and intimate interfacial contact, the heterostructured $BaTiO_3@TiO_2$ exhibits much more efficiency than $BaTiO_3/TiO_2$ physical mixtures. The facilitation of this unique structure on RhB decomposition is ascribed to the polarization-induced built-in electric field generated in $BaTiO_3$. The built-in electric field can penetrate the interfacial region and TiO_2 shell to drive the separation of photo-induced charge carriers, reduce the recombination rate of the electrons and holes, and then degrade the pollutants effectively. The calculated degradation rates of RhB are shown in Figure 6(b), where the $BaTiO_3@TiO_2$ possesses the largest degradation rate due to the accelerated separation of photo-induced carriers determined by the interfacial built-in electric field.

The cycling stability of photocatalysts was also characterized by investigating their cyclic property using the catalysts of pure TiO_2, $BaTiO_3/TiO_2$ physical mixtures and $BaTiO_3@TiO_2$ nanohybrids. Thus, four cyclic experiments were conducted to clarify the photo-catalytic activity and stability under UV light. A series of absorption spectra of RhB solution are portrayed in Figure 7. For all three catalysts, the intensity of the maximum absorption peak of RhB solution at 554 nm weakens under the application of UV irradiation, indicating a rapid decomposition of RhB solution during 120 min. The insets of Figures 7(a), (c) and (e) show the color change of RhB with different irradiation time, which fades gradually after undergoing 120 min. The photocatalytic activity and stability of $BaTiO_3@TiO_2$ nanohybrids are much higher than that of pure TiO_2 or $BaTiO_3/TiO_2$ physical mixtures; the degradation efficiency increases from 44% to 52%, 33% to 40%, and 20% to 23%, which indicate that the degradation efficiency decreased by 14%, 10% and 3% for pure TiO_2, $BaTiO_3/TiO_2$ physical mixtures and $BaTiO_3@TiO_2$ nanohybrids, respectively. In spite of the increase in photocatalytic activity, the cycling stability of $BaTiO_3@TiO_2$ is improved obviously under UV irradiation, after four cycles of photocatalytic, only 3% decrease in photocatalytic activity. These results demonstrate the built-in field generated in heterostructured $BaTiO_3@TiO_2$ can maintain photo-induced carrier separation preferable. Simple physical mixing of photocatalyst and TiO_2 has been employed to improve the photocatalytic efficiency; however, the momentary random collision of heterophase particles induces the poor electron transfer characteristic and limit enhancement of photocatalytic efficiency [34]. Furthermore, the constructed heterostructure of physical mixtures tends to be destroyed in the solution.

The semiconductor photocatalysis process mainly contains generation and transportation of charge carriers under light irradiation, which would further react with water to induce actives including hydroxyl radicals (OH•) and superoxide anions ($\bullet O_2^-$) to decompose organic pollutants. Suppressing charge recombination and improving carrier transport by ferroelectric polarization-induced built-in electric field was designed in this work. The separation of carriers is promoted because the built-in electric field can penetrate the TiO_2 when its thickness is less than the depletion width (~100 nm). Taking the depletion width of 100 nm, the built-in electric field approved by SSPFM is 40 V/μm, which is consistent with the built-in electric field estimated by adopting the classical dipole field model in our previous study [26]. Figure 8 illustrates a schematic of the polarization-induced built-in electric field in charge separation and transfer. The enhancement of photocatalytic activities of $BaTiO_3@TiO_2$ is attributed to the accelerating separation of carriers, which are driven by the built-in field force generated by spontaneous polarization. The charge carriers tend to transfer

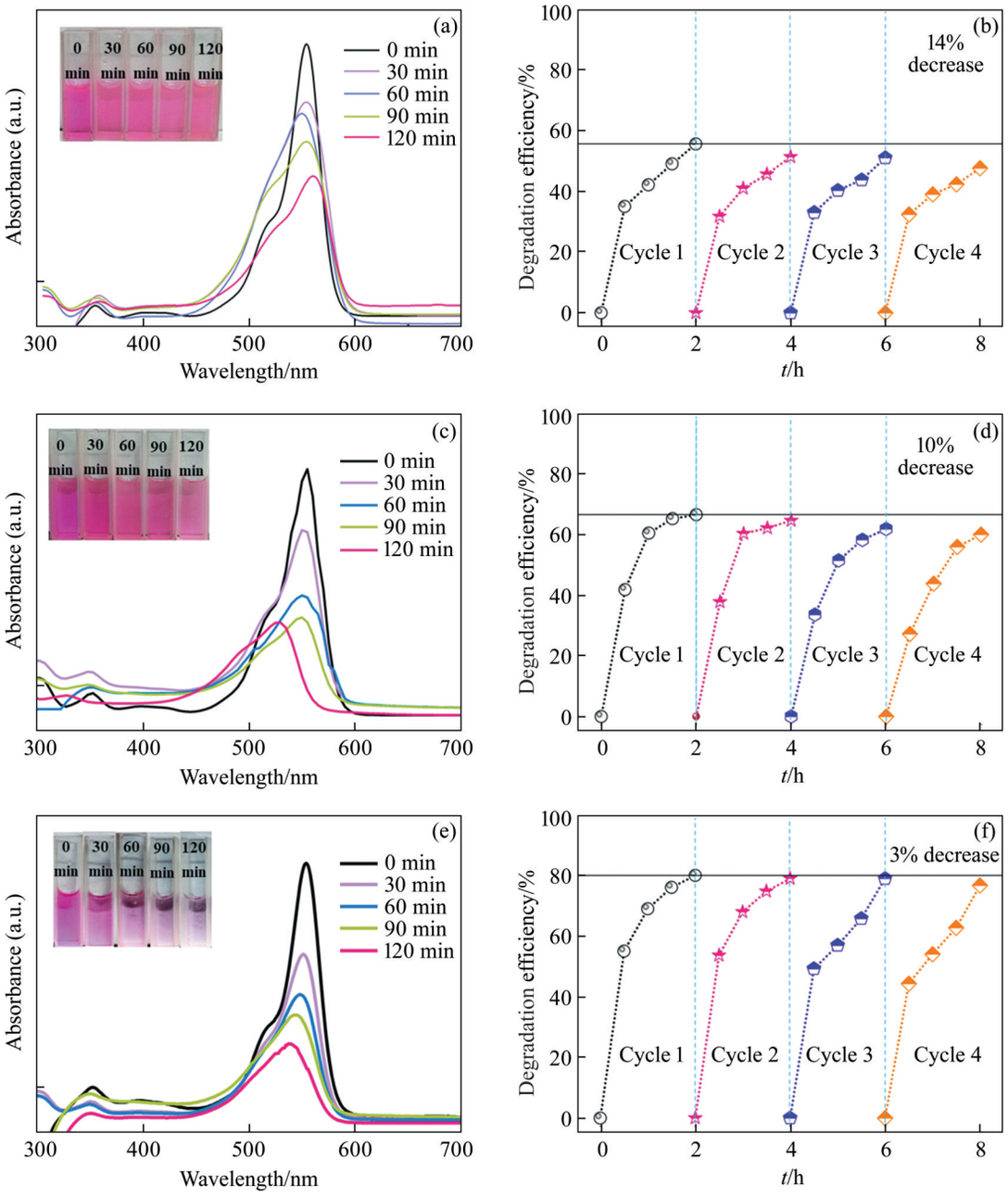

Figure 7 Absorption spectra (a, c, e) of RhB solution under UV irradiation and their cyclic degradation curves (b, d, f) in the presence of (a, b)TiO_2, (c, d) $BaTiO_3$/TiO_2 physical mixtures and (e, f) heterostructured $BaTiO_3$@TiO_2(The insets in Figures 7 (a, c, e) display the color change of RhB solution during the photocatalysis process)

through the interface of heterostructured photocatalyst. Thus, the thickness of TiO_2 and the size of interface contact area become the key-point for photocatalytic activity. As shown in Figure 8, heterostructured $BaTiO_3$@TiO_2 nanoparticles showed good dispersion and large contact area. By contrast, nanosized $BaTiO_3$ and mesoporous TiO_2 tend to aggregate and form ball-liked clusters in $BaTiO_3$/TiO_2 physical mixtures. The agglomeration will reduce the interfacial contact area and induce large quantities of electrons and holes recombination. Furthermore, TiO_2 with large size dimension (430 nm) is not beneficial for penetration of the built-in electric field, and thus the enhancement of photocatalytic activity is limited. Therefore, the interface structure and interfacial interaction greatly affect the efficiency of charges transfer and separation, which in turn determine the photocatalytic efficiency of the heterostructured photocatalyst.

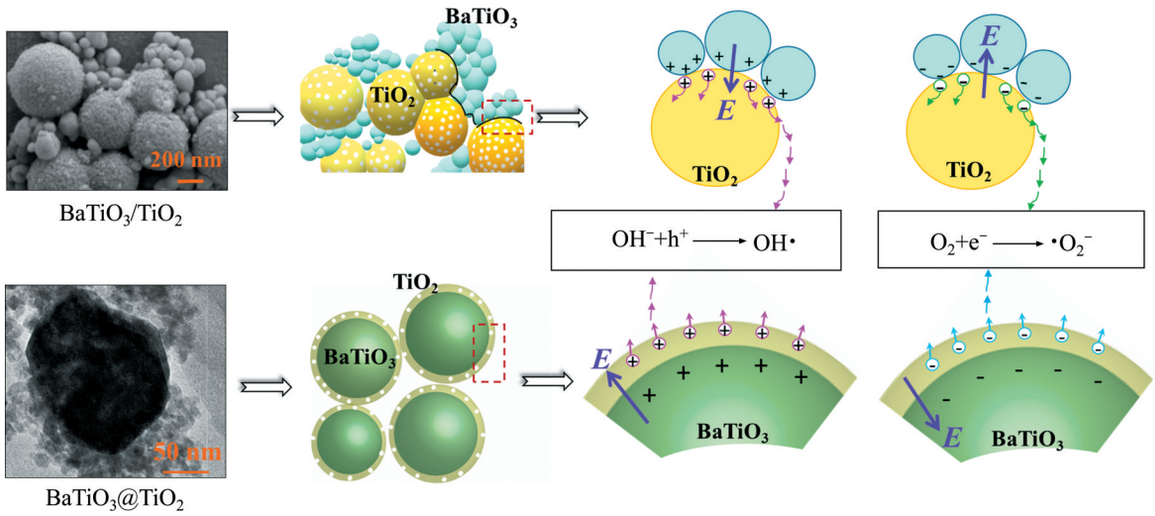

Figure 8 Schematic illustration of built-in electric field in charge separation and transport of $BaTiO_3/TiO_2$ physical mixtures and heterostructured $BaTiO_3@TiO_2$

4 Conclusions

In summary, we have designed a heterostructured hybrid photocatalyst by hydrothermally coating mesoporous TiO_2 onto the surface of ferroelectric $BaTiO_3$ nanoparticles. The heterostructured $BaTiO_3@TiO_2$ exhibits significantly improved photocatalytic activity and photostability in organic pollutants degradation. The improvements in photocatalytic performance are ascribed to the synergistic effect of polarization-induced built-in electric field generated by $BaTiO_3$, the high photocatalytic activity of mesoporous TiO_2 and the intimate interfacial contacts. The interface structure and interfacial interaction affect the built-in electric field greatly, and further influence the separation and transfer of charge carriers, which result in improving photocatalytic efficiency. Coupled with the simplicity and scalability of preparation, this work provides an efficient route to develop heterostructured photocatalysts with high photocatalytic activity by rational manipulation of interfacial interactions.

Contributors

FAN Bao-yan and LIU Xiao-yan provided the concept and edited the draft of manuscript. LIU Hai-bo conducted the literature review and wrote the first draft of the manuscript. WANG Zhen-hui, ZHAO Yi-wen, YANG Sen, and LYU Si-yi conducted experiments and provided relevant data. XING An and ZHANG Jun analyzed the measured data. FAN Bao-yan, LI He and LIU Xiao-yan edited the draft of manuscript and revised the final version.

Conflict of interest

FAN Bao-yan, LIU Hai-bo, WANG Zhen-hui, ZHAO Yi-wen, YANG Sen, LYU Si-yi, XING An, ZHANG Jun, LI He and LIU Xiao-yan declare that they have no conflict of interest.

References

[1] ISMAIL M, WU Zheng, ZHANG Luo-hong, MA Jiang-ping, JIA Yan-min, HU Yong-ming, WANG Yao-jin. High-efficient synergy of piezocatalysis and photocatalysis in bismuth oxychloride nanomaterial for dye decomposition [J]. Chemosphere, 2019, 228: 212 – 218. DOI: 10.1016/j.chemosphere.2019.04.121.

[2] MA Jiang-ping, REN Jing, JIA Yan-min, WU Zheng, CHEN Lin, HAUGEN N O, HUANG Hai-tao, LIU Yong-sheng. High efficiency bi-harvesting light/vibration energy using piezoelectric zinc oxide nanorods for dye decomposition [J]. Nano Energy, 2019, 62: 376 – 383. DOI: 10.1016/j. nanoen. 2019.05.058.

[3] HAN Fang, KAMBALA V S R, SRINIVASAN M, RAJARATHNAM D, NAIDU R. Tailored titanium dioxide photocatalysts for the degradation of organic dyes in wastewater treatment: A review [J]. Applied Catalysis A: General, 2009, 359(1, 2): 25 – 40. DOI: 10.1016/j. apcata. 2009.02.043.

[4] WANG Huan-wei, FANG Xin, WAN Yu-chi, ZHAN Jing, WANG Zhi-jian, LIU Hua. Visible-lightinduced $NiCo_2O_4@Co_3O_4$ core/shell heterojunction photocatalysts for efficient removal of organic dyes [J]. Journal of Central

South University, 2021, 28(10): 3040−3049. DOI: https://doi.org/10.1007/s11771-021-4793-8.

[5] YANG Bian, WU Chao, WANG Jian-wei, BIAN Ji-hong, WANG Lei, LIU Ming, DU Ya-ping, YANG Yao-dong. When C_3N_4 meets $BaTiO_3$: Ferroelectric polarization plays a critical role in building a better photocatalyst [J]. Ceramics International, 2020, 46(4): 4248 − 4255. DOI: 10.1016/j.ceramint.2019.10.145.

[6] LEI Hua, ZHANG Huan-huan, ZOU Yan, DONG Xiao-ping, JIA Yan-min, WANG Fei-fei. Synergetic photocatalysis/piezocatalysis of bismuth oxybromide for degradation of organic pollutants [J]. Journal of Alloys and Compounds, 2019, 809: 151840. DOI: 10.1016/j.jallcom.2019.151840.

[7] WANG J, TAFEN N, LEWIS J P, HONG Z, MANIVANNAN A, ZHI M, LI M, WU N. Origin of photocatalytic activity of nitrogen-doped TiO_2 nanobelts [J]. Journal of the American Chemical Society, 2009, 131(34): 12290−12297. DOI: 10.1021/ja903781h.

[8] SINGH S, FARAZ M, KHARE N. Recent advances in semiconductor-graphene and semiconductor-ferroelectric/ferromagnetic nanoheterostructures for efficient hydrogen generation and environmental remediation [J]. ACS Omega, 2020, 5(21): 11874−11882. DOI: 10.1021/acsomega.9b03913.

[9] TAN Xu, ZHOU Shan, TAO Hui-jin, WANG Wei-yang, WAN Qiang-wei, ZHANG Ke-chen. Influence of Ag on photocatalytic performance of Ag/ZnO nanosheet photocatalysts [J]. Journal of Central South University, 2019, 26(7): 2011−2018. DOI: https://doi.org/10.1007/s11771-019-4148-x.

[10] JIN Lin-feng, CHAI Li-yuan, SONG Ting-ting, YANG Wei-chun, WANG Hai-ying. Preparation of magnetic Fe_3O_4@Cu/Ce microspheres for efficient catalytic oxidation co-adsorption of arsenic(III) [J]. Journal of Central South University, 2020, 27(4): 1176 − 1185. DOI: 10.1007/s11771-020-4358-2.

[11] YAO Shun-yu, ZHANG Xu, QU Feng-yu, UMAR A, WU Xiang. Hierarchical WO_3 nanostructures assembled by nanosheets and their applications in wastewater purification [J]. Journal of Alloys and Compounds, 2016, 689: 570 − 574. DOI: 10.1016/j.jallcom.2016.08.025.

[12] NING Xiao-feng, LU Gong-xuan. Photocorrosion inhibition of CdS-based catalysts for photocatalytic overall water splitting [J]. Nanoscale, 2020, 12(3): 1213 − 1223. DOI: 10.1039/c9nr09183a.

[13] WU Fei, YU Yan-hao, YANG Huang, et al. Simultaneous enhancement of charge separation and hole transportation in a TiO_2-$SrTiO_3$ core-shell nanowire photoelectrochemical system [J]. Advanced Materials, 2017, 29(28): 1701432. DOI: 10.1002/adma. 201701432.

[14] ZHANG Jing, XU Qian, FENG Zhao-chi, LI Mei-jun, LI Can. Importance of the relationship between surface phases and photocatalytic activity of TiO_2 [J]. Angewandte Chemie International Edition, 2008, 47(9): 1766 − 1769. DOI: 10.1002/anie.200704788.

[15] YANG Nai-liang, LIU Yuan-yuan, WEN Hao, TANG Zhi-yong, ZHAO Hui-jun, LI Yu-liang, WANG Dan. Photocatalytic properties of graphdiyne and graphene modified TiO_2: From theory to experiment [J]. ACS Nano, 2013, 7(2): 1504−1512. DOI: 10.1021/nn305288z.

[16] LI Shun, LIN Yuan-hua, ZHANG Bo-ping, LI Jing-feng, NAN Ce-wen. $BiFeO_3$/TiO_2 core-shell structured nanocomposites as visible-active photocatalysts and their optical response mechanism [J]. Journal of Applied Physics, 2009, 105(5): 054310. DOI: 10.1063/1.3091286.

[17] CUI Yong-fei, BRISCOE J, WANG Ya-qiong, TARAKINA N V, DUNN S. Enhanced photocatalytic activity of heterostructured ferroelectric $BaTiO_3$/α-Fe_2O_3 and the significance of interface morphology control [J]. ACS Applied Materials & Interfaces, 2017, 9(29): 24518 − 24526. DOI: 10.1021/acsam.

[18] LI Li, LIU Xuan, ZHANG Yi-ling, SALVADOR P A, ROHRER G S. Heterostructured (Ba, Sr)TiO_3/TiO_2 core/shell photocatalysts: Influence of processing and structure on hydrogen production [J]. International Journal of Hydrogen Energy, 2013, 38(17): 6948 − 6959. DOI: 10.1016/j.ijhydene.2013.03.130.

[19] LI Li, ROHRER G S, SALVADOR P A. Heterostructured ceramic powders for photocatalytic hydrogen production: Nanostructured TiO_2 shells surrounding microcrystalline (ba, Sr)TiO_3 cores [J]. Journal of the American Ceramic Society, 2012, 95(4): 1414 − 1420. DOI: 10.1111/j. 1551-2916.2012.05076.x.

[20] FENG Ke-yuan, LIU Xiao-yan, SI Dong-hui, TANG Xiao, XING An, OSADA M, XIAO Peng. Ferroelectric $BaTiO_3$ dipole induced charge transfer enhancement in dye-sensitized solar cells [J]. Journal of Power Sources, 2017, 350: 35 − 40. DOI: 10.1016/j.jpowsour.2017.03.049.

[21] YANG W, YU Y, STARR M B, YIN X, LI Z, KVIT A, WANG S, ZHAO P, WANG X. Ferroelectric polarization-enhanced photoelectrochemical water splitting in TiO_2-$BaTiO_3$ core-shell nanowire photoanodes [J]. Nano Letters, 2015, 15(11): 7574 − 7580. DOI: 10.1021/acs. nanolett.5b03988.

[22] HUANG Han-jie, LI Dan-zhen, LIN Qiang, SHAO Yu, CHEN Wei, HU Yin, CHEN Yi-bin, FU Xian-zhi. Efficient photocatalytic activity of PZT/TiO_2 heterojunction under visible light irradiation [J]. The Journal of Physical Chemistry C, 2009, 113(32): 14264 − 14269. DOI: 10.1021/jp902330w.

[23] WANG Z, SONG J, GAO F, SU R, ZHANG D, LIU Y, XU C, LOU X, YANG Y. Developing a ferroelectric nanohybrid for enhanced photocatalysis [J]. Chemical Communications (Cambridge, England), 2017, 53(54): 7596 − 7599. DOI: 10.1039/c7cc02548c.

[24] SU E C, HUANG Bing-shun, LEE J T, WEY M Y. Excellent dispersion and charge separation of $SrTiO_3$-TiO_2 nanotube derived from a two-step hydrothermal process for facilitating hydrogen evolution under sunlight irradiation [J]. Solar Energy, 2018, 159: 751 − 759. DOI: 10.1016/j. solener. 2017.11.048.

[25] KOO Y S, SONG K M, HUR N, et al. Strain-induced magnetoelectric coupling in $BaTiO_3$/Fe_3O_4 core/shell nanoparticles [J]. Applied Physics Letters, 2009, 94(3): 032903. DOI: 10.1063/1.3073751.

[26] GUAN B Y, GUAN B Y, YU L, LI J, LOU X W. A universal cooperative assembly-directed method for coating of mesoporous TiO_2 nanoshells with enhanced lithium storage properties [J]. Science Advances, 2016, 2(3): e1501554. DOI: 10.1126/sciadv.1501554.

[27] LIU X Y, LV S, FAN B Y, XING A, JIA B. Ferroelectric

polarization-enhanced photocatalysis in $BaTiO_3$-TiO_2 core-shell heterostructures [J]. Nanomaterials (Basel, Switzerland), 2019, 9(8): E1116. DOI: 10.3390/nano9081116.

[28] HAFID L, GODEFROY G, EL IDRISSI A, MICHEL-CALENDINI F. Absorption spectrum in the near U. V. and electronic structure of pure Barium titanate [J]. Solid State Communications, 1988, 66(8): 841−845. DOI: 10.1016/0038-1098(88)90397-3.

[29] HURUM D C, AGRIOS A G, GRAY K A, RAJH T, THURNAUER M C. Explaining the enhanced photocatalytic activity of degussa P25 mixed-phase TiO_2 using EPR [J]. The Journal of Physical Chemistry B, 2003, 107(19): 4545−4549. DOI: 10.1021/jp0273934.

[30] POLKING M J, HAN M G, YOURDKHANI A, et al. Ferroelectric order in individual nanometre-scale crystals [J]. Nature Materials, 2012, 11(8): 700 − 709. DOI: 10.1038/nmat3371.

[31] GUO Jia-qi, ZHU Zhe, QUAN Hua-feng, DUAN Wen-jiu, GAO Ju. Domain switchings within $BaTiO_3$ nanofibers under different polarizing voltages and loading forces [J]. Ceramics International, 2017, 43(3): 3113 − 3117. DOI: 10.1016/j.ceramint.2016.11.125.

[32] CHEN J, LU Hai-dong, LIU H J, CHU Ying-hao, DUNN S, (KEN) OSTRIKOV K, GRUVERMAN A, VALANOOR N. Interface control of surface photochemical reactivity in ultrathin epitaxial ferroelectric films [J]. Applied Physics Letters, 2013, 102(18): 182904. DOI: 10.1063/1.4802885.

[33] LIU Guang-qing, CHEN J, LICHTENSTEIGER C, TRISCONE J M, AGUADO-PUENTE P, JUNQUERA J, VALANOOR N. Positive effect of an internal depolarization field in ultrathin epitaxial ferroelectric films [J]. Advanced Electronic Materials, 2016, 2(1): 1500288. DOI: 10.1002/aelm.201500288.

[34] YANG Chong-yin, WANG Wen-deng, SHAN Zhi-chao, HUANG Fu-qiang. Preparation and photocatalytic activity of high-efficiency visible-light-responsive photocatalyst SnS_x/TiO_2 [J]. Journal of Solid State Chemistry, 2009, 182(4): 807−812. DOI: 10.1016/j.jssc.2008.12.018.

(Edited by YANG Hua)

中文导读

界面工程调控铁电极化增强异质结构$BaTiO_3$@TiO_2光催化性能

摘要：采用水解沉淀结合水热法成功合成光催化活性增强的铁电-$BaTiO_3$@光电-TiO_2纳米杂化光催化剂($BaTiO_3$@TiO_2)。与纯 TiO_2、纯 $BaTiO_3$ 和 $BaTiO_3$/TiO_2机械混合物相比，采用异质结构的$BaTiO_3$@TiO_2降解罗丹明B (RhB)的光催化活性和循环稳定性得到提升，其光催化降解效率是纯 TiO_2 的 1.7 倍，纯 $BaTiO_3$ 的 7.2 倍。光催化降解效率的提升与光电TiO_2、铁电$BaTiO_3$及两者界面结构的协同效应相关。介孔微结构的TiO_2因高的比表面积而具备优异的光催化活性。纳米$BaTiO_3$因铁电极化产生的内建电场及$BaTiO_3$与TiO_2间紧密的界面相互作用而有效地促进光生载流子的分离和传输。通过调控界面工程将促进具有优异光催化性能异质结型光催化剂的设计与开发。

关键词：异质结型$BaTiO_3$@TiO_2；铁电极化；界面相互作用；光催化活性